

First-principles study of the polar (111) surface of Fe_3O_4

L. Zhu,^{1,*} K. L. Yao,^{1,2,†} and Z. L. Liu^{1,3}¹*Department of Physics, Huazhong University of Science and Technology, Wuhan 430074, China*²*International Center of Materials Physics, The Chinese Academy of Science, Shenyang 110015, China*³*State Key Laboratory of Coordination Chemistry, Nanjing University, Nanjing 210093, China*

(Received 26 October 2005; revised manuscript received 30 January 2006; published 10 July 2006)

We performed a systematic full-potential density functional theory study with the generalized gradient and local density approximation+ U approaches on five possible (1×1) terminations of the low-index polar (111) surface of Fe_3O_4 . Applying the concepts of first-principles thermodynamics, we analyze the composition, the structure, and the stability of the Fe_3O_4 (111) orientation at equilibrium with an arbitrary oxygen environment. The densities of states of the unrelaxed and relaxed Fe_3O_4 (111) surfaces were calculated and compared with that of bulk Fe_3O_4 . The calculations reveal that the $\text{Fe}_{\text{oct}2}$ - $\text{Fe}_{\text{tet}1}$ -O1-terminated surface is energetically favored, showing metallic properties. The $\text{Fe}_{\text{oct}1}$ -O2-terminated surface is more active than the other two Fe-terminated surfaces, showing half-metallic properties, similar to bulk Fe_3O_4 . The $\text{Fe}_{\text{tet}1}$ -O1-terminated surface, the O-terminated surfaces, and the surfaces with vacancy defects all show metallic properties.

DOI: 10.1103/PhysRevB.74.035409

PACS number(s): 68.47.De, 68.47.Fg, 73.20.At, 75.70.Rf

I. INTRODUCTION

Metal oxides with strong electronic correlations are of great interest due to their technologically important uses, such as catalysis, magnetic data storage, high-temperature superconductivity, and the colossal magnetoresistive materials.¹⁻⁴ To obtain a microscopic understanding of these compounds, it is necessary to know their surface atomic structure. A lot of research has been done for polar surfaces of different materials by using the density functional theory. They all used thin atomic layers to simulate a semi-infinite truncation surface, and obtained good results.⁵⁻⁸ Magnetite (Fe_3O_4) is important in geophysics and mineralogy, and it is also attracting increasing attention as a potential material for spintronic devices, due to the predicted half-metallic behavior⁹ and the high Curie temperature of 858 K.

Magnetite has the inverse spinel crystal structure based on a fcc lattice of oxygen (O^{2-}) anions, containing Fe cations in tetrahedrally (so-called A sites) and octahedrally (B sites) coordinated interstices, with close-packed O planes lying perpendicular to the [111] direction. The A sites are occupied by Fe^{3+} ions and the B sites are occupied half by Fe^{3+} ions and half by Fe^{2+} ions.¹⁰ Along the [111] direction, there are two types of iron sublayers, one with all octahedrally coordinated Fe atoms, and the other with octahedrally and tetrahedrally coordinated Fe atoms alternating between cubic close-packed oxygen sublayers. The stacking sequence along the [111] direction can be schematically represented by $\text{Fe}_{\text{tet}1}$ -O1- $\text{Fe}_{\text{oct}1}$ -O2- $\text{Fe}_{\text{tet}2}$ - $\text{Fe}_{\text{oct}2}$ - $\text{Fe}_{\text{tet}1}$ -O1, as shown in Fig. 1(a). Here the subscripts tet1 and tet2 refer to fourfold-coordinated Fe layers, and oct1 and oct2 correspond to Fe layers where the iron atoms are sixfold coordinated to O atoms. O1 and O2 correspond to cubic close-packed O sublayers. In the Fe_3O_4 (111)- (1×1) unit cell, each cubic close-packed O sublayer comprises four oxygen atoms. Figure 1(b) presents a top view with the Fe_3O_4 (111)- (1×1) unit cell. Here each letter denotes the lateral registry of the two-dimensional (1×1) unit cell containing four oxygen atoms as indicated in the top view. The four-O monolayer splits into

two monolayers, which are about 0.04 Å apart. Three oxygen atoms are symmetrically equivalent (O_b) and coordinated to one top-layer iron atom, while the single O_a atom is not. The surface of magnetite has been studied intensively over the past decade, as it is a very interesting material for spintronics. It is one of the few materials with a very high degree of spin polarization at the Fermi level. Spintronics almost invariably involves electron transport across or along a material interface. Therefore, an understanding of the structure and the electronic properties of the surfaces and interfaces is a key issue for making progress in this area. At the same time, progress on exploring the potential of magnetite

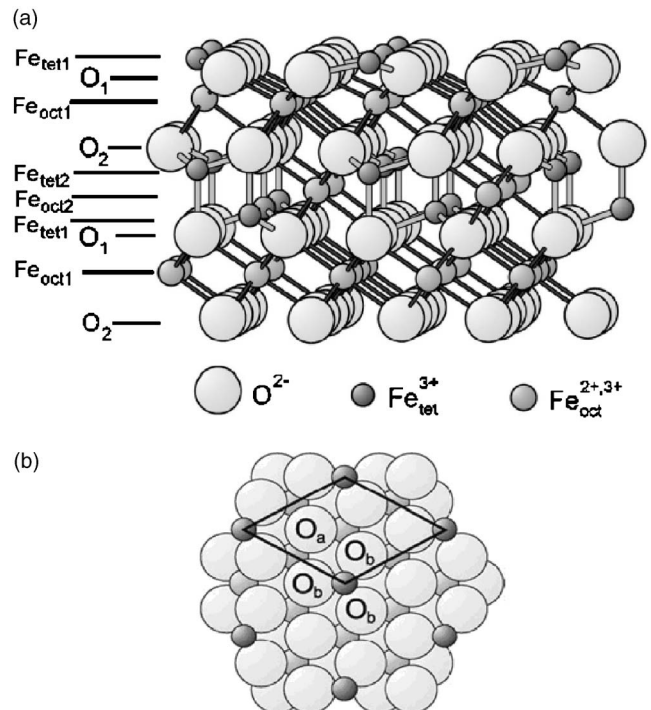


FIG. 1. (a) Side view of the Fe_3O_4 (111) surface structure. (b) Top view of the Fe_3O_4 (111)- (1×1) unit cell.

for spintronics is slowed by the complexity of the magnetite structure. Magnetite has six possible bulk terminations in the [111] direction.¹¹ Two of them represent terminations consisting of close-packed oxygen layers, and the other four are surface planes containing cations (Fe^{2+} , Fe^{3+}). There are significant differences among the four Fe terminations. One of them, consisting of Fe tetrahedral sites, is arranged in a hexagonal (honeycomb) lattice with a 6 Å periodicity ($\text{Fe}_{\text{tet1}}\text{-O}$).¹²⁻¹⁴ Another one has octahedral-site Fe atoms and is arranged in a Kagome lattice with 3 Å interatomic distances ($\text{Fe}_{\text{oct1}}\text{-O}$). The two others, with octahedral and tetrahedral iron layers are separated by 0.6 Å in the [111] direction (such as $\text{Fe}_{\text{oct2}}\text{-Fe}_{\text{tet1}}\text{-O}$).¹⁵ One of the two oxygen terminations appears as an oxygen monolayer on top of the octahedral Fe, while the other one covers a multilayer of tetrahedral and octahedral Fe atoms.¹⁶ The surface is highly sensitive to the preparation conditions. Moreover, self-consistent band structure calculations of the magnetite surface and surface reconstruction models for low-index terminations are still not available.

In this paper, we have studied five of these six bulk terminations of the Fe_3O_4 (111) surface. They are the $\text{Fe}_{\text{tet1}}\text{-O1}$ -, $\text{Fe}_{\text{oct1}}\text{-O2}$ -, $\text{Fe}_{\text{oct2}}\text{-Fe}_{\text{tet1}}\text{-O1}$ -, $\text{O1-Fe}_{\text{oct1}}$ -, and $\text{O2-Fe}_{\text{tet2}}$ -terminated surfaces. The vacancy defect of the surface is considered in the calculation.

II. COMPUTATIONAL METHOD

The calculations were performed in the framework of density functional theory (DFT). We use the full-potential augmented-plane-wave (FP APW) method in the WIEN2K package.¹⁷ The optimized calculation of the lattice constants is carried out with the generalized gradient approximation (GGA),¹⁸ and the calculation of the total energy and the analysis of the electronic structure are all done by using the self-interaction-corrected (SIC) local density approximation^{19,20} (LDA) with electron correlation (LDA + U). In this LDA + U (SIC) method, the strong correlation between localized d electrons is explicitly taken into account through the screened effective electron-electron interaction parameter U_{eff} , which is an empirical parameter with the physical background of the Hubbard model. Usually, the Hubbard-like U_{eff} is evaluated by comparison of the theoretically calculated energy positions of energy bands with x-ray photoemission spectroscopy and ultraviolet photoemission spectroscopy measurements. However, the U_{eff} term is difficult to calculate accurately since it depends on the covalency of the system.²¹ As a consequence, the U term may vary for the same element in different polymorphs, and needs to be fitted for each structure under investigation. In our case, we have two types of Fe ions in Fe_3O_4 with different occupation numbers for their $3d$ shells. Obviously, the effective repulsion of $3d$ electrons described by U_{eff} depends on the number of holes in the $3d$ shell (the ionicity), and U_{eff} should increase with increasing ionicity.²² The estimation in Ref. 9 gave the value of the on-site Coulomb interaction parameter for the Fe(B) site equal to 4.1 ± 0.5 eV. Constrained calculations²³ with two types of charge ordering gave $U_{\text{eff}} = 4.5$ eV. The LDA + U band structure calculations with U_{eff}

varying from 4 to 6 eV provide optical, magneto-optical, and x-ray magnetic circular dichroism spectra in reasonable agreement with the experimental data. On the other hand, the value of the energy gap strongly depends on the value of U_{eff} . We have also justified the U_{eff} values within the full-potential linearized augmented-plane-wave (FPLAPW) method for bulk Fe_3O_4 . The calculated value of U_{eff} depends on theoretical approximations and for our purposes it is sufficient to regard the value of U_{eff} as a parameter; we try to ascertain its value from comparison of the calculated physical properties of Fe_3O_4 with experiments. We set the U_{eff} to 4.0 and 4.5 eV for the Fe(B)- and Fe(A)-site ions, respectively. These U_{eff} values also have been used for Fe(B)- and Fe(A)-site ions in bulk Fe_3O_4 by Antonov *et al.*,^{24,25} and they got a good result. All the parameters chosen are consistent during calculations. By electronic structure calculations using the LDA + U method we have obtained a periodic charge disproportion along the c axis in bulk Fe_3O_4 . The proposed charge ordering is in good agreement with the one derived from experiment.²⁶ Calculations for the total energy of the surface slab and analysis of the electronic structure are all carried out using the spin-polarized implementation.

In this paper, the self-consistent field calculations are based on the following parameters: the atomic-sphere radii R_{MT} are chosen as 2.0 and 1.0 a.u. for the Fe and O atoms, respectively. With the DFT GGA approach the optimized lattice constant (a_0) for the cubic bulk Fe_3O_4 is 8.41 Å and the u parameter is 0.0046, in good agreement with the experimental values²⁷ of 8.394 Å and 0.0048. The optimized lattice constant of the Fe_3O_4 (111)-(1 × 1) surface is $a=b=5.932$ Å, which is also in good agreement with the experimental value of 5.92 Å. Inside the muffin tins (MTs) the wave functions are expanded in spherical harmonics up to $l_{\text{max}}^{\text{wf}}=12$, and the nonspherical contributions to the electron density and potential are considered up to $l_{\text{max}}^{\text{pot}}=6$. The charge density Fourier expansion cutoff $G_{\text{max}}=14$ in the muffin tins; 300 k points in the first Brillouin zone were adopted

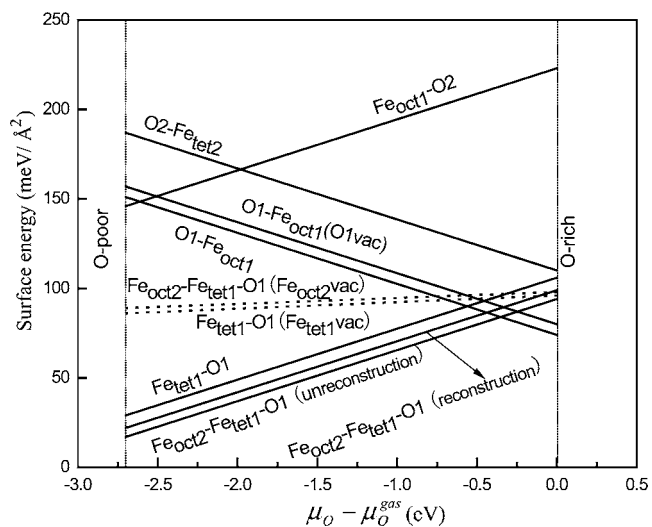


FIG. 2. Calculated surface free energy $\gamma(T, P)$ as a function of the chemical potential of oxygen $\mu_{\text{O}} - \mu_{\text{O}}^{\text{gas}}$ (eV) for all studied terminations. The dotted vertical lines indicate the allowed range of the oxygen chemical potential.

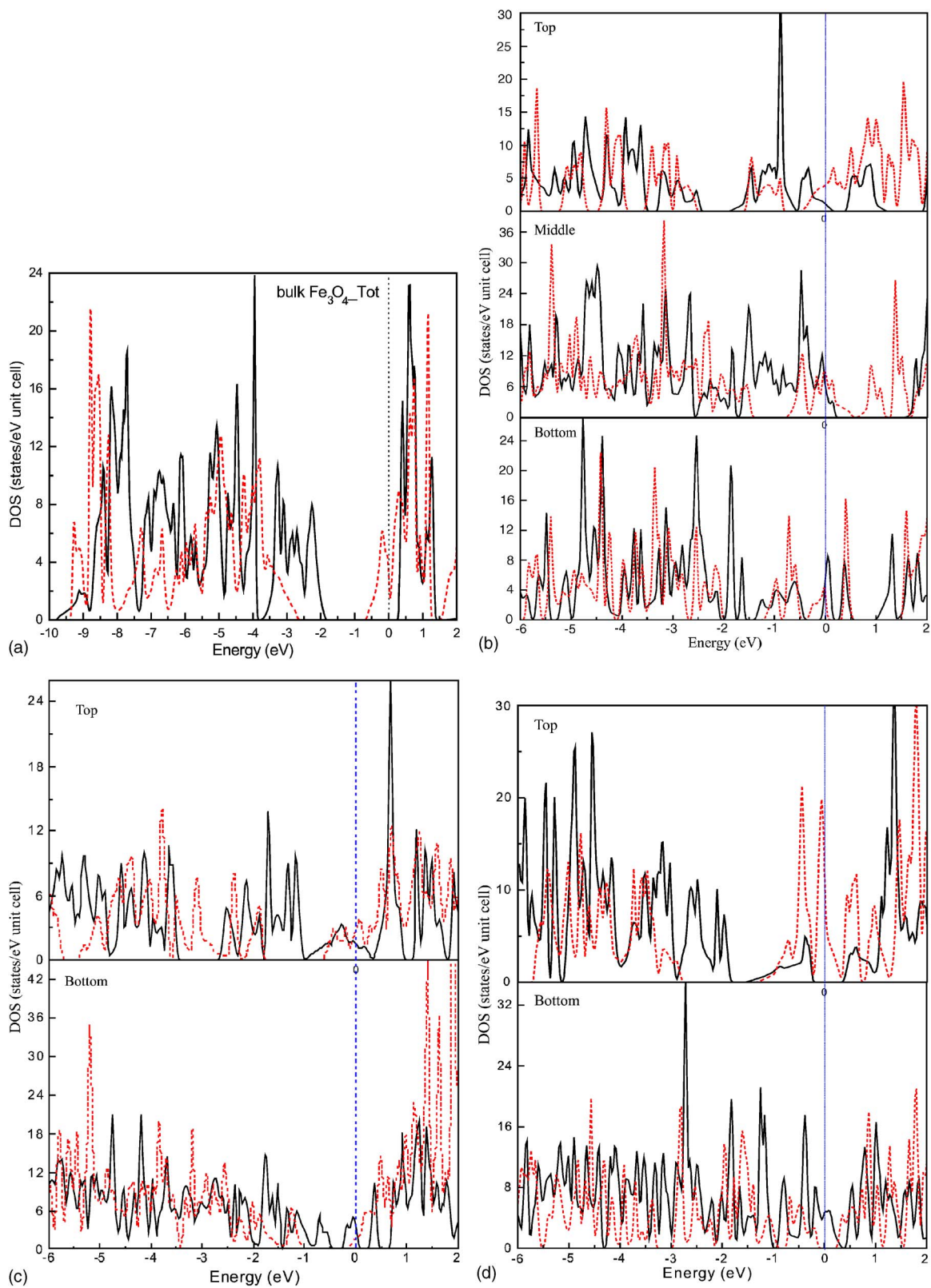


FIG. 3. (Color online) Total density of states (DOS) of bulk Fe_3O_4 and the Fe-terminated Fe_3O_4 (111) unrelaxed and relaxed surfaces: (a) bulk Fe_3O_4 , (b) $\text{Fe}_{\text{oct}2}\text{-Fe}_{\text{tet}1}\text{-O1}$ -terminated surface (top, unrelaxed surface; middle, relaxed but unreconstructed surface; bottom, relaxed and reconstructed surface), (c) $\text{Fe}_{\text{tet}1}\text{-O1}$ -terminated surface (top, unrelaxed surface; bottom, relaxed and reconstructed surface), and (d) $\text{Fe}_{\text{oct}1}\text{-O2}$ -terminated surface (top, unrelaxed surface; bottom, relaxed and reconstructed surface). The solid and dotted lines denote the majority and the minority spins, respectively. The Fermi levels are located at 0 eV.

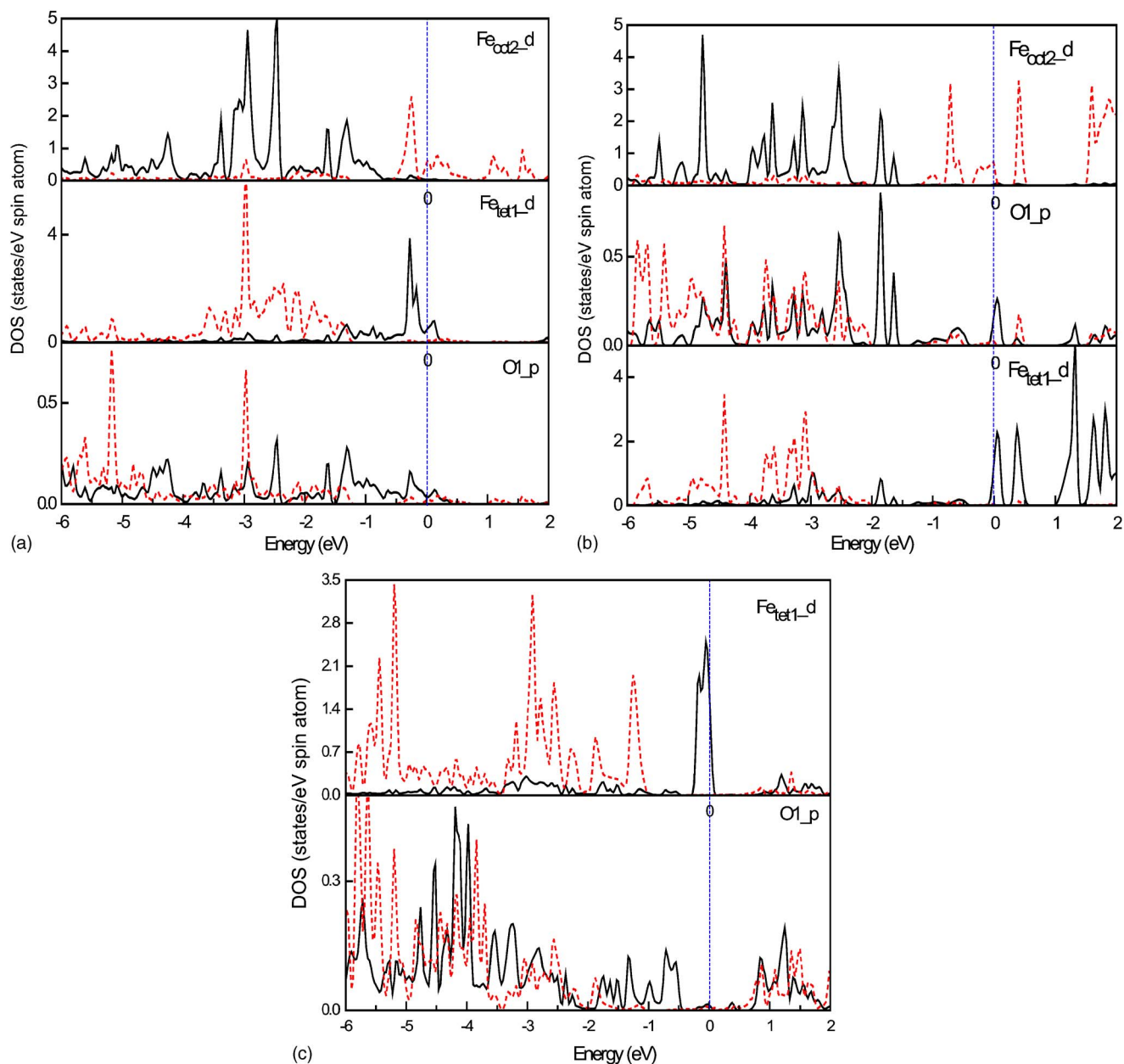


FIG. 4. (Color online) Partial density of states for (a) the $\text{Fe}_{\text{oct}2}\text{-Fe}_{\text{tet}1}\text{-O1}$ -terminated surface (unreconstructed) (the Fe atoms are in the topmost layer; O1 is next to the topmost Fe layer); (b) the $\text{Fe}_{\text{oct}2}\text{-Fe}_{\text{tet}1}\text{-O1}$ -terminated surface (reconstructed) (the $\text{Fe}_{\text{oct}2}$ atoms are in the topmost layer, O1 is next to the topmost Fe layer, $\text{Fe}_{\text{tet}1}$ is under the second sublayers of oxygen); (c) the $\text{Fe}_{\text{tet}1}\text{-O1}$ -terminated surface (top, $3d$ states of $\text{Fe}_{\text{tet}1}$ in the topmost layer; bottom, $2p$ states of O1 next to the topmost Fe layer). The solid and dotted lines denote the majority and the minority spins, respectively. The Fermi levels are located at 0 eV.

in the calculations (243 points in the irreducible part of the surface Brillouin zone) with 241 899 plane waves at the equilibrium lattice constant. The cutoff parameter $R_{\text{MT}}K_{\text{max}}$ limiting the number of plane waves is equal to 5.0, where K_{max} is the maximal value of the reciprocal lattice vector used in the plane-wave expansion, and R_{MT} is the smallest atomic-sphere radius in the surface cell, so the plane-wave cutoff energy is 340 eV. With these cutoff parameters an accuracy of energy differences better than 0.1 meV has been achieved.

III. RESULTS OF SURFACE CALCULATIONS

To simulate the (111) surface of Fe_3O_4 , we use supercells containing 13–19 atomic planes; the vacuum is used in the simulations, the vacuum between the repeated slabs amounting to 10 Å. We have restricted the calculations to structures compatible with a (1×1) cell and some surfaces to (2×2) supercells. First, we expose the two surfaces of the slab to the vacuum; then we carry out a full geometry optimization of the two surfaces of the slab, and both surfaces converge to the same geometry. The relaxation is complete; all atoms of

the slab are allowed to relax and no symmetry restrictions are applied. After optimization, it is found that four of the five bulk terminations of the Fe_3O_4 (111) surface are unreconstructed but strongly relaxed. Dynamical low-energy electron diffraction and scanning tunneling microscopy image analysis also show these surfaces are unreconstructed but relaxed.^{13–15} It is found that the outmost atomic layers of the Fe_{oct1} -O2-terminated surface are switched. After optimization, the Fe_{oct1} -O2-terminated surface becomes an O2-terminated surface. The optimized interlayer relaxations as percentages of the corresponding bulk values and the interlayer spacings for the five Fe_3O_4 (111) relaxed slabs are shown in Table I, and are compared with the bulk values (experimental values²⁸ on the left-hand side and calculated values on the right-hand side). The relaxed interlayer spacings of the Fe_{tet1} -O1-terminated surface are compared with Ref. 14 (experimental values on the left-hand side and calculated values on the right-hand side). According to the optimized calculation, we find that the coordination of the atoms on the surface of Fe_3O_4 (111) slab has been reduced relative to that of the bulk, the atoms moving inward to strengthen their interaction with the atoms of the sublayer. The defect considered in our calculation is that one of the outmost atoms is vacant. We have also fixed the bottom 6–14 atomic planes at their ideal bulk position and fully relaxed the outermost 5–8 upper atomic layers. From the results, we find that the Fe_{tet1} -O1-terminated surface, the Fe_{oct1} -O2-terminated surface, the O1- Fe_{oct1} -terminated surface, and the O2- Fe_{tet2} -terminated surface have similar relaxations with simultaneous full geometry optimization of the two surfaces of the slab, and the outmost atomic layers of the Fe_{oct1} -O2-terminated surface are also switched. As for the Fe_{oct2} - Fe_{tet1} -O1-terminated surface we also find that the surface layer are rearranged, as shown in Table II. The reconstruction induces a switch in the upper layers. Therefore, the ordering of the layers from the surface toward the bulk is as follows: first, a single layer of octahedral iron atoms coordinated to the three atoms O_b of the layer beneath; the atoms O_a come next and the tetrahedral iron layer is the fourth layer, close to the empty site of the dense layer.

In order to compare the relative stability of structures containing different numbers of atoms, we consider different surfaces in contact with an oxygen atmosphere described by oxygen pressure P and temperature T . The most stable surface composition is the one that minimizes the surface free energy $\gamma(T, P)$,²⁹

$$\gamma(T, P) = \frac{1}{A} [E_{\text{tot}} - N_{\text{Fe}}\mu_{\text{Fe}}(T, P) - N_{\text{O}}\mu_{\text{O}}(T, P)]. \quad (1)$$

Here, E_{tot} is the total energy of the slab, N_{Fe} and N_{O} are the numbers of Fe and O atoms in the supercell, and μ_{Fe} and μ_{O} are the chemical potentials of the Fe atom and the O atom, respectively. However, if there is enough bulk material to act as a thermodynamic reservoir, the potentials are in fact no longer independent, but are related to the Gibbs free energy of the bulk oxide,

$$3\mu_{\text{Fe}}(T, P) + 4\mu_{\text{O}}(T, P) = g_{\text{Fe}_3\text{O}_4}^{\text{bulk}}(T, P),$$

where g is used to denote the Gibbs free energy per formula unit. The Gibbs free energies can be approximated by the internal energies $E(T=0, P=0, N_{\text{Fe}}, N_{\text{O}})$ from DFT (DFT + U) calculations. Inserting this constraint into Eq. (1) leads to

$$\gamma(T, P) = \frac{1}{A} \left[E_{\text{tot}} - \frac{1}{3} N_{\text{Fe}} g_{\text{Fe}_3\text{O}_4}^{\text{bulk}}(T, P) + \left(\frac{4}{3} N_{\text{Fe}} - N_{\text{O}} \right) \mu_{\text{O}}(T, P) \right]. \quad (2)$$

This surface energy depends on the total energy of the slab, the slab stoichiometry, and the oxygen chemical potential. To determine the surface stability in an oxygen atmosphere, the surface energy calculated for different surface terminations (i.e., different slab stoichiometries) is plotted against the oxygen chemical potential. The termination with the lowest energy is the stable surface at this oxygen partial pressure.

The elemental Fe or O chemical potential must be less than the corresponding bulk chemical potential; otherwise, the element would form the energetically more favorable bulk structure. That is to say,

$$\mu_{\text{Fe}} \leq \mu_{\text{Fe}(\text{bulk})}, \quad \mu_{\text{O}} \leq \mu_{\text{O}(\text{bulk})}. \quad (3)$$

Therefore, this μ_{O} can be varied within certain boundaries. The lower boundary for μ_{O} , which will be called the O-poor limit, is defined by the decomposition of the oxide into iron and oxygen. A reasonable upper boundary for μ_{O} , on the other hand (O-rich limit), is given by gas-phase conditions that are so oxygen rich that O condensation will start on the sample at a low enough temperature. Therefore, the range of the O chemical potential is

$$\Delta G_f(0, 0) \leq \mu_{\text{O}} - \mu_{\text{O}}^{\text{gas}} \leq 0, \quad (4)$$

where $\Delta G_f = \mu_{\text{Fe}_3\text{O}_4(\text{bulk})} - 3\mu_{\text{Fe}(\text{bulk})} - 4\mu_{\text{O}(\text{gas})}$ is the 0 K formation heat of the bulk Fe_3O_4 . The O chemical potential is referenced with respect to the total energy of an oxygen molecule. $\Delta\mu_{\text{O}} = \mu_{\text{O}} - \mu_{\text{O}}^{\text{gas}} = \mu_{\text{O}} - (1/2)E_{\text{O}_2}^{\text{total}}$. To consider the uncertainty in these theoretically well-defined but approximate limits for $\Delta\mu_{\text{O}}$, we will always plot the dependence of the surface free energies some tenths of an eV outside these boundaries. From this it will be shown below that the uncertainty in the boundaries does not affect at all our physical conclusions.

The results for the surface energy as a function of the oxygen chemical potential according to Eq. (2) are shown in Fig. 2. From Fig. 2, we can see that the Fe-terminated surfaces are more stable than the O-terminated surfaces at low oxygen chemical potential $\mu_{\text{O}} - \mu_{\text{O}}^{\text{gas}}$. At the allowed oxygen chemical potential, the surface free energy of the Fe_{oct1} -O2-terminated surface is higher than those of the other two Fe-terminated surfaces over the whole range. A surface with large surface energy is in a rather unfavorable state, that is to say, the Fe_{oct1} -O2-terminated surface is more active than the other two Fe-terminated surfaces, and the Fe_{oct2} - Fe_{tet1} -O1-terminated surface is energetically favored. This result is consistent with that found by Ahdjoudj *et al.* and Noguera,^{11,30} who confirmed that the stability of the

TABLE I. Optimized calculation of the interlayer relaxations and the interlayer spacings for Fe_3O_4 (111) relaxed slabs compared with the bulk values (experimental values on the left-hand side, taken from Ref. 14 for the $\text{Fe}_{\text{tet}1}$ -O1-terminated slab and from Ref. 28 for the bulk, and calculated values on the right-hand side) when the two surfaces of the slab are fully optimized.

$\text{Fe}_{\text{tet}1}$ -O1 terminated Layer distance (\AA) (Relaxation) (%)	$\text{Fe}_{\text{oct}2}$ - $\text{Fe}_{\text{tet}1}$ -O1 terminated Layer distance (\AA) (Relaxation) (%)	O1- $\text{Fe}_{\text{oct}1}$ terminated Layer distance (\AA) (Relaxation) (%)
$\text{Fe}_{\text{tet}1}$	$\text{Fe}_{\text{oct}2}$	3O_b
0.38 ± 0.05 0.37	\uparrow 0.23	\uparrow 0.14
$(-41 \pm 7) \downarrow$ (-41)	\downarrow (-62)	\downarrow
3O_b	$\text{Fe}_{\text{tet}1}$	1O_a
0.08 ± 0.09 0.10	\uparrow 0.40	\uparrow 0.77
\downarrow	\downarrow (-36)	\downarrow (-32)
1O_a	3O_b	$\text{Fe}_{\text{oct}1}$
0.87 ± 0.05 0.82	\uparrow 0.13	\uparrow 1.15
$(-26 \pm 4) \downarrow$ (-28)	\downarrow	\downarrow (+1)
$\text{Fe}_{\text{oct}1}$	1O_a	1O_a
1.36 ± 0.05 1.28	\uparrow 0.91	\uparrow 0.12
$(+15 \pm 4) \downarrow$ (+12)	\downarrow (-20)	\downarrow
3O_b	$\text{Fe}_{\text{oct}1}$	3O_b
0.12 ± 0.09 0.14	\uparrow 1.03	\uparrow 0.49
\downarrow	\downarrow (-10)	\downarrow (-22)
1O_a	1O_a	$\text{Fe}_{\text{tet}2}$
0.57 ± 0.05 0.52	\uparrow 0.05	\uparrow 0.95
$(-11 \pm 7) \downarrow$ (-17)	\downarrow	\downarrow (+56)
$\text{Fe}_{\text{tet}2}$	3O_b	$\text{Fe}_{\text{oct}2}$
	\uparrow 0.54	\uparrow 0.31
	\downarrow (-14)	\downarrow (-49)
	$\text{Fe}_{\text{tet}2}$	$\text{Fe}_{\text{tet}1}$
O2- $\text{Fe}_{\text{tet}2}$ terminated	$\text{Fe}_{\text{oct}1}$ -O2 terminated	Bulk
Layer distance (\AA)	Layer distance (\AA)	Layer distance (\AA)
(Relaxation) (%)	(Reconstruction)	(Relaxation) (%)
1O_a	3O_b	$\text{Fe}_{\text{oct}2}$
\uparrow 0.06	\uparrow 0.02	$0.606 \uparrow 0.606$
\downarrow	\downarrow	\downarrow
3O_b	1O_a	$\text{Fe}_{\text{tet}1}$
\uparrow 0.37	\uparrow 0.26	$0.626 \uparrow 0.629$
\downarrow (-41)	\downarrow	\downarrow
$\text{Fe}_{\text{tet}2}$	$\text{Fe}_{\text{oct}1}$	3O_b
\uparrow 0.42	\uparrow 0.629	$0.04 \uparrow 0.047$
\downarrow (-30)	\downarrow	\downarrow
$\text{Fe}_{\text{oct}2}$	$\text{Fe}_{\text{tet}2}$	1O_a
\uparrow 0.80	\uparrow 0.996	$1.154 \uparrow 1.14$
\downarrow (+32)	\downarrow	\downarrow
$\text{Fe}_{\text{tet}1}$	$\text{Fe}_{\text{tet}1}$	$\text{Fe}_{\text{oct}1}$
\uparrow 0.52	\uparrow 0.198	$1.154 \uparrow 1.14$
\downarrow (-18)	\downarrow	\downarrow
3O_b	$\text{Fe}_{\text{oct}2}$	1O_a
\uparrow 0.11	\uparrow 0.720	$0.04 \uparrow 0.047$
\downarrow	\downarrow	\downarrow
1O_a	3O_b	3O_b

TABLE I. (Continued.)

Fe _{tet1} -O1 terminated Layer distance (Å) (Relaxation) (%)	Fe _{oct2} -Fe _{tet1} -O1 terminated Layer distance (Å) (Relaxation) (%)	O1-Fe _{oct1} terminated Layer distance (Å) (Relaxation) (%)
↑ 1.12	↑ 0.14	0.626 ↑ 0.629
↓ (-2)	↓	↓
Fe _{oct1}	1O _a	Fe _{tet2}
	↑ 1.011	0.606 ↑ 0.606
	↓	↓
	Fe _{oct1}	Fe _{oct2}

slabs depends on the overall composition, specifically on the deviation from stoichiometry, and on the dipole moment perpendicular to the surface. An *ab initio* Hartree-Fock study in a slab geometry¹¹ predicted that termination by an iron bilayer (Fe_{oct2}/Fe_{tet1}/4O/... sequence) is energetically favored, due to exchange of iron and oxygen layers in the slab. We have also found a similar switch of oxygen and Fe(tetrahedral) in an Fe_{oct2}-Fe_{tet1}-O1-terminated slab as shown in Table II. The switch allows the positive charges of the ferrous and ferric ions to be distributed on both sides of the first oxygen layer, which reduces the local dipole perpendicular to the surface. In Ref. 11, it is suggested that the stability of an Fe-monolayer-terminated slab (Fe_{tet1}/4O/... sequence) can be enhanced by adsorption of hydrogen. The O1-Fe_{oct1}-terminated surface is more stable than the Fe-terminated surface at high oxygen chemical potential $\mu_O - \mu_O^{\text{gas}}$. As the oxygen chemical potential $\mu_O - \mu_O^{\text{gas}}$ increases, the O1-Fe_{oct1}-terminated surface gradually becomes more stable, because when the oxygen pressure increases, the dipole moment of the Fe-terminated surface increases, but the dipole moment of the O-terminated surface decreases. We believe that decreasing the spacing between the Fe and O layers reduces both the length of the total dipole and the charges borne by the atoms, which stabilize these polar surfaces. The relative surface energies of the relaxed surfaces and that of the unrelaxed slab show very large differences. After relaxation, the surface energies decrease a lot. The change of coordination and the subsequent reduction of the Madelung potential also induce surface stability.

The stabilization and the large relaxation of the Fe₃O₄ (111) surface are connected with strong changes of the electronic and magnetic properties. To understand the electronic nature of these surfaces, we have calculated the density of states (DOS) of the unrelaxed and relaxed (111) surfaces. In the bulk, magnetite shows a half-metallic behavior with a band gap in the majority-spin channel of approximately 0.5 eV and 100% spin polarization due to the t_{2g} states of Fe(B) at E_F in the majority-spin channel.¹ Figure 3 shows the total density of states of the bulk Fe₃O₄ and the total DOS of Fe-terminated Fe₃O₄ (111) unrelaxed and relaxed surfaces, where the plotted energy range is from -6.0 to 2.0 eV and the Fermi level is set to zero. The densities of states of the unrelaxed and relaxed slabs have a similar character, which does not depend strongly on the absolute

values of the interlayer relaxation. From Fig. 3, one can see that the Fe_{oct2}-Fe_{tet1}-O1- and the Fe_{tet1}-O1-terminated surfaces and their outmost Fe vacancy surfaces with relaxation and unrelaxation all have metallic properties. That is to say, there is no longer a gap in the density of states for minority-spin electrons and the system is transformed to a normal-metal state due to the surface structure. But the Fe_{oct1}-O2-terminated surfaces with relaxation and unrelaxation have half-metallic properties, similar to bulk Fe₃O₄. The O-terminated and O-terminated O-vacancy surfaces with relaxation and unrelaxation all have metallic properties, consistent with the results found by Berdunov *et al.*³¹ It is known that in transition metals the 3d electrons make a large contribution to the tunneling current. In the case of O- and Fe-terminated surfaces, one might not expect a tunneling contribution from the oxygen p states. However, on the surface the hybridization between oxygen p states and transition metal d states changes the situation by altering the oxygen p orbitals from insulating to conductive.³² Figure 4 depicts the atom-projected partial DOSs of the first two or three atom layers of the Fe_{oct2}-Fe_{tet1}-O1-terminated surface (unreconstruction), the Fe_{oct2}-Fe_{tet1}-O1-terminated surface (reconstruction), and the Fe_{tet1}-O1-terminated surface. The layer-projected partial density of states in Fig. 4 shows significant p - d state hybridization between the topmost Fe ions and the oxygen anions in the layer underneath. The p states of the oxygen anions are shifted to the Fermi level, eliminating the band gap. The p states of the outmost oxygen of the O-terminated surface also contribute to the tunneling current. The modification of the surface electronic structure, the total and partial filling of surface states, destroys the electrostatic instability.

Bulk magnetite is a ferrimagnet with the magnetic moments of tetrahedral iron ($-3.94\mu_B$) and octahedral iron ($3.83\mu_B$) oriented antiparallel to each other and a total magnetic moment of 4.0 per formula unit. The magnetic moments of Fe atoms are all calculated by the LDA+ U in our study. Without applying the LDA+ U , the magnetic moments of tetrahedral and octahedral iron in bulk Fe₃O₄ are $3.53\mu_B$ and $3.46\mu_B$, respectively. In the FL APW method, the unit cell is divided into two parts: (1) nonoverlapping atomic spheres (centered at the atomic sites) and (2) an interstitial region. If we chose the radius of the atom large enough, but without overlapping of the sphere atoms, the magnetic moment will be almost all from the atoms, and the contribution

TABLE II. As for Table I, with the bottom atomic planes fixed at their ideal bulk positions.

Fe _{tet1} -O1 terminated Layer distance (Å) (Relaxation) (%)	Fe _{oct1} -Fe _{tet1} -O1 terminated Layer distance (Å) (Reconstruction)	O1-Fe _{oct1} terminated Layer distance (Å) (Relaxation) (%)
Fe _{tet1}	Fe _{oct2}	3O _b
0.38±0.05 0.33	↑ 0.59	↑ 0.03
(-41±7)↓ (-47)	↓	↓
3O _b	3O _b	1O _a
0.08±0.09 0.17	↑ 0.13	↑ 0.69
↓	↓	↓ (-39)
1O _a	1O _a	Fe _{oct1}
0.87±0.05 0.86	↑ 0.96	↑ 1.04
(-26±4)↓ (-25)	↓	↓ (-9)
Fe _{oct1}	Fe _{tet1}	1O _a
1.36±0.05 1.31	↑ 0.81	↑ 0.23
(+15±4)↓ (+15)	↓	↓
3O _b	Fe _{oct1}	3O _b
0.12±0.09 0.13	↑ 0.91	↑ 0.59
↓	↓	↓ (-6)
1O _a	1O _a	Fe _{tet2}
0.57±0.05 0.56	↑ 0.05	↑ 0.82
-11±7 ↓ (-11)	↓	↓ (+30)
Fe _{tet2}	3O _b	Fe _{oct2}
	↑ 0.26	↑ 0.35
	↓	↓ (-42)
	Fe _{tet2}	Fe _{tet1}
O2-Fe _{tet2} terminated	Fe _{oct1} -O2 terminated	Bulk
Layer distance (Å)	Layer distance (Å)	Layer distance (Å)
(Relaxation) (%)	(Reconstruction)	(Relaxation) (%)
1O _a	3O _b	Fe _{oct2}
↑ 0.06	↑ 0.24	0.606 ↑ 0.606
↓	↓	↓
3O _b	1O _a	Fe _{tet1}
↑ 0.31	↑ 0.23	0.626 ↑ 0.629
↓ (-51)	↓	↓
Fe _{tet2}	Fe _{oct1}	3O _b
↑ 0.44	↑ 0.46	0.04 ↑ 0.047
↓ (-27)	↓	↓
Fe _{oct2}	Fe _{tet2}	1O _a
↑ 0.79	↑ 1.20	1.154 ↑ 1.14
↓ (+30)	↓	↓
Fe _{tet1}	Fe _{tet1}	Fe _{oct1}
↑ 0.59	↑ 0.25	1.154 ↑ 1.14
↓ (-6)	↓	↓
3O _b	Fe _{oct2}	1O _a
↑ 0.03	↑ 0.46	0.04 ↑ 0.047
↓	↓	↓
1O _a	3O _b	3O _b
↑ 0.96	↑ 0.21	0.626 ↑ 0.629
↓ (-16)	↓	↓
Fe _{oct1}	1O _a	Fe _{tet2}

TABLE II. (Continued.)

Fe _{tet1} -O1 terminated Layer distance (Å) (Relaxation) (%)	Fe _{oct1} -Fe _{tet1} -O1 terminated Layer distance (Å) (Reconstruction)	O1-Fe _{oct1} terminated Layer distance (Å) (Relaxation) (%)
	↑ 0.93	0.606 ↑ 0.606
	↓	↓
	Fe _{oct1}	Fe _{oct2}

from the interstitial region is very small. In our case, the atomic-sphere radii R_{MT} are chosen as 2.0 and 1.0 a.u for the Fe and O atoms, respectively. The magnetic moment is also affected significantly by the correlation energy U . The difference of the magnetic moments between results considering and not considering U is almost $0.41\mu_B$ per Fe atom in the bulk Fe_3O_4 . When U is added, the magnetic moment of the Fe atom is increased. After relaxation, the magnetic moment of the surface Fe atoms is substantially reduced due to the strong relaxations. In the Fe-terminated surface, the magnetic moment of the outmost Fe(A) is about $-3.36\mu_B$ and the magnetic moment of the outmost Fe(B) is about $3.24\mu_B$. The magnetic moment of the other subsurface Fe is close to that of the bulk. Additionally, a substantial magnetic moment of approximately $0.23\mu_B$ is induced in the undercoordinated surface oxygen with a missing bond to iron, while the magnetic moments of the rest of the surface oxygen atoms are close to those of the bulk, $0.07\mu_B$. A similar magnetization was also observed for the Fe_3O_4 (001) and oxygen-terminated $\alpha-Fe_2O_3$ (0001) surfaces.^{4,33}

IV. CONCLUSIONS

We have performed *ab initio* calculations by employing density functional theory with the GGA and LDA+ U approaches to determine the structure of Fe_3O_4 (111) surfaces at equilibrium with an oxygen environment. The surface free energies of the five possible (111) surfaces of Fe_3O_4 were calculated. Different structures with periodicity (1×1) were fully optimized. According to our calculation, it is found that the Fe_{oct2}-Fe_{tet1}-O1-terminated surface is energetically favored and has metallic properties. The Fe_{oct1}-O2-terminated surface has half-metallic properties, similar to bulk Fe_3O_4 . The Fe_{oct2}-Fe_{tet1}-O1-terminated surface, the O-terminated surfaces, and the surfaces with vacancy defects all show metallic properties.

ACKNOWLEDGMENTS

This work was supported by the National Natural Science Foundation of China under Grants No. 10574047 and No. 10574048. The authors thank L. Zhao for valuable suggestions.

*Corresponding author. FAX: 0086-27-87544525. Electronic address: wl-zl41@163.com

†Electronic address: klyao@hust.edu.cn

¹Y. J. Kim, C. Westphal, R. X. Ynzunza, H. C. Galloway, M. Salmeron, M. A. Van Hove, and C. S. Fadley, Phys. Rev. B **55**, R13448 (1997).

²X. W. Zhou, H. N. G. Wadley, J.-S. Filhol, and M. N. Neurock, Phys. Rev. B **69**, 035402 (2004).

³S.-R. Liu, Z. Dohnalek, R. S. Smith, and B. D. Kay, J. Phys. Chem. B **108**, 3644 (2004).

⁴R. Pentcheva, F. Wendler, H. L. Meyerheim, W. Moritz, N. Jedrecy, and M. Scheffler, Phys. Rev. Lett. **94**, 126101 (2005).

⁵C. Cheng, Phys. Rev. B **71**, 052401 (2005).

⁶A. Rohrbach, J. Hafner, and G. Kresse, Phys. Rev. B **70**, 125426 (2004).

⁷Y. L. Li, K. L. Yao, Z. L. Liu, and G. Y. Gao, Phys. Rev. B **72**, 155446 (2005).

⁸M. Fonin, R. Pentcheva, Yu. S. Dedkov, M. Sperlich, D. V. Vylikh, M. Scheffler, U. Rüdiger, and G. Güntherodt, Phys. Rev. B **72**, 104436 (2005).

⁹Z. Zhang and S. Satpathy, Phys. Rev. B **44**, 13319 (1991).

¹⁰R. Cornell and U. Schwertmann, *The Iron Oxides* (Verlagsgesellschaft, Cambridge, U.K., 1996).

¹¹J. Ahdjoudj, C. Martinsky, C. Minot, M. A. Van Hove, and G. A. Somorjai, Surf. Sci. **443**, 133 (1999).

¹²W. Weiss, A. Barbieri, M. A. Van Hove, and G. A. Somorjai, Phys. Rev. Lett. **71**, 1848 (1993).

¹³A. Barbieri, W. Weiss, M. A. Van Hove, and G. A. Somorjai, Surf. Sci. **302**, 259 (1994).

¹⁴M. Ritter and W. Weiss, Surf. Sci. **432**, 81 (1999).

¹⁵A. R. Lennie, N. G. Condon, F. M. Leibsle, P. W. Murray, G. Thornton, and D. J. Vaughan, Phys. Rev. B **53**, 10244 (1996).

¹⁶N. Berdunov, S. Murphy, G. Mariotto, and I. V. Shvets, Phys. Rev. B **70**, 085404 (2004).

¹⁷P. Blaha, K. Schwarz, Georg K. H. Madsen, D. Kvasnicka, and J. Luitz, Computer code WIEN2K (Techn. Universit Wien, Austria, 2001).

¹⁸J. P. Perdew, K. Burke, and M. Ernzerhof, Phys. Rev. Lett. **77**, 3865 (1996).

¹⁹I. I. Mazin and V. I. Anisimov, Phys. Rev. B **55**, 12822 (1997).

²⁰V. I. Anisimov, J. Zaanen, and O. K. Andersen, Phys. Rev. B **44**, 943 (1991).

²¹M. S. Hybertsen, M. Schlüter, and N. E. Christensen, Phys. Rev. B **39**, 9028 (1989).

²²V. N. Antonov, A. N. Yaresko, A. Ya. Perlov, P. Thalmeier, P. Fulde, P. M. Oppeneer, and H. Eschrig, Phys. Rev. B **58**, 9752

- (1998).
- ²³V. I. Anisimov, I. S. Elfimov, N. Hamada, and K. Terakura, *Phys. Rev. B* **54**, 4387 (1996).
- ²⁴V. N. Antonov, B. N. Harmon, V. P. Antropov, A. Ya. Perlov, and A. N. Yaresko, *Phys. Rev. B* **64**, 134410 (2001).
- ²⁵V. N. Antonov and B. N. Harmon, *Phys. Rev. B* **67**, 024417 (2003).
- ²⁶J. P. Wright, J. P. Attfield, and P. G. Radaelli, *Phys. Rev. B* **66**, 214422 (2002).
- ²⁷W. Hamilton, *Phys. Rev.* **110**, 1050 (1958).
- ²⁸R. W. G. Wyckoff, in *Crystal Structures*, 2nd ed. (Krieger Publishing Co., Malabar, FL, 1982), Vol. 2, p. 5.
- ²⁹K. Reuter and M. Scheffler, *Phys. Rev. B* **65**, 035406 (2002).
- ³⁰Claudine Noguera, *J. Phys.: Condens. Matter* **12**, R367 (2000).
- ³¹N. Berdunov, S. Murphy, G. Mariotto, and I. V. Shvets, *Phys. Rev. Lett.* **93**, 057201 (2004).
- ³²E. Y. Tsymbal, O. N. Mryasov, and P. R. LeClair, *J. Phys.: Condens. Matter* **15**, R109 (2003).
- ³³X.-G. Wang, W. Weiss, Sh. K. Shaikhutdinov, M. Ritter, M. Petersen, F. Wagner, R. Schlögl, and M. Scheffler, *Phys. Rev. Lett.* **81**, 1038 (1998).